

Columbia University
in the City of New York

**DEPARTMENT OF CIVIL ENGINEERING
AND ENGINEERING MECHANICS**



Ground Characteristics and Free Field Strains

by

M. Shinozuka

and

H. Kawakami

August 1977

Technical Report No. CU-2

Prepared for

**The National Science Foundation
under Grant No. ENV-76-09838**

**Reproduction in whole or in part is permitted for any purpose
of the United States Government.**

REPORT DOCUMENTATION PAGE		1. REPORT NO. NSF/RA-770786	2.	3. Recipient's Accession No. PB298150	
4. Title and Subtitle Ground Characteristics and the Free Field Strains				5. Report Date August 1977	
7. Author(s) M. Shinozuka, H. Kawakami				8. Performing Organization Rept. No. Technical Report No CU-2	
9. Performing Organization Name and Address Columbia University Department of Civil Engineering and Engineering Mechanics New York, New York 10027				10. Project/Task/Work Unit No.	
12. Sponsoring Organization Name and Address Engineering and Applied Science (EAS) National Science Foundation 1800 G Street, N.W. Washington, D.C. 20550				11. Contract(C) or Grant(G) No. (C) (G) ENV7609838	
15. Supplementary Notes				13. Type of Report & Period Covered Technical	
16. Abstract (Limit: 200 words) Elastic shear strains in the non-homogeneous surface layer subjected to incident shear waves have been evaluated using a quasi-two-dimensional analysis. The shear strains arise from the randomly non-homogeneous property of a surface layer subjected to vertically incident shear waves emanating through the semi-infinite firm ground underneath. Shear strains produced by different incident shear waves have been computed for the root mean square (RMS) values for the metropolitan Tokyo area on the basis of local soil conditions. A reasonable correlation was established between such normal strains and the statistics collected on the underground water supply pipelines under the 1923 Kanto Earthquake. Mathematical formulas, diagrams, data tabulations, charts, and numerous references are included.					
17. Document Analysis a. Descriptors					
Soil mechanics		Elastic waves		Pipelines	
Soil dynamics		Shear properties		Water supply	
b. Identifiers/Open-Ended Terms					
Tokyo		Shear waves			
Free field status		Elastic shear strains			
c. COSATI Field/Group					
18. Availability Statement NTIS		19. Security Class (This Report)		21. No. of Pages 37	
		20. Security Class (This Page)		22. Price R 703/MF01	

Capital Systems Group, Inc.

CAPITAL SYSTEMS GROUP, INC.
6110 EXECUTIVE BOULEVARD
SUITE 250
DALLAS, TEXAS 75248

Foreword

This technical report represents an immediate continuation of the work described in "Underground Pipe Damages and Ground Characteristics" by the present authors published as Technical Report CU-1 prepared for the National Science Foundation under Grant No. ENV-76-09838 and presented at the Lifeline Earthquake Engineering Specialty Conference at the University of California, Los Angeles, August 30 - 31, 1977. For the convenience of the readers, however, an effort has been made to make this report self-contained as much as possible. Because of this, some duplication of the material with Technical Report No. CU-1 has occurred. When the results of these two reports are combined in the near future for the purpose of publication in a technical journal as a single paper, these duplications will be eliminated.

Any opinions, findings, conclusions or recommendations expressed in this publication are those of the author(s) and do not necessarily reflect the views of the National Science Foundation.

Abstract

A quasi-two-dimensional analysis method proposed in Ref. 1 has been extended to evaluate the elastic shear strains arising from spatial variability of the soil property of a surface layer subjected to shear waves incident vertically from below through a semi-infinite firm ground. Applying the method, the root mean square (RMS) values of the shear strains are evaluated for the metropolitan Tokyo area on the basis of the local soil conditions, and the correlation between such RMS values and the statistics of the damage collected on the underground water supply pipelines under the 1923 Kanto Earthquake has been examined.

1. Introduction

In a previous work¹, describing the spatial variability of the soil property, particularly that of the ground predominant frequency as a random function of space variable characterized by mean value, variance and correlation distance, a quasi-two-dimensional analysis was performed to determine the normal strains in the surface layer subjected to a shear wave incident vertically from below through a semi-infinite firm ground as shown in Fig. 1. The analysis was applied to the metropolitan Tokyo area and a reasonable correlation was established between such normal strains and the statistics collected on the damage of the underground water supply pipelines under the 1923 Kanto Earthquake.

The displacement in the surface layer considered in Ref. 1 is due to a shear wave S_0 incident vertically from below in such a way that the soil particle motions are in the direction of the x-axis producing the normal strain

$$\epsilon_0 = \partial u / \partial x \quad (1)$$

The same shear wave also gives rise to the shear strain

$$\gamma_0 = \partial u / \partial z \quad (2)$$

in the x-z plane.

One can also consider the case, however, where the surface layer is subjected to an incident shear wave S_1 at its interface with the firm ground which again propagates vertically from below but with the particle motion in the direction of the y-axis. In this case, the shear strain γ_1 is produced in the

x-y plane;

$$\gamma_1 = \partial v / \partial x \quad (3)$$

as well as the shear strain γ_1'

$$\gamma_1' = \partial v / \partial z \quad (3a)$$

in the y-z plane where the x-y-z axes constitute a right-handed rectangular Cartesian coordinate system with corresponding displacement components u, v, and w as shown in Fig. 2.

Fig. 3 shows schematically the incident shear waves S_0 and S_1 when they are sinusoidal.

The analysis developed here as well as in Ref. 1 places an emphasis on the fact that the strain ϵ_0 and γ_1 are not identically equal to zero solely because the soil property of the surface layer is (randomly) nonhomogeneous. In fact, Ref. 1 has shown that the normal strain ϵ_0 resulting from the nonhomogeneity can be considerably large, although at present such nonhomogeneity is generally considered to produce a significant effect only under extremely unusual circumstances and is dealt with qualitatively if indeed dealt with. Also, the following observations appear to be in order: Currently, one usually associates, for design purposes, normal strains in the x-direction with the plane P-wave while shear and bending strains in the x-z or x-y plane with the plane S-wave, both propagating either in the direction of the x-axis or in the oblique direction with respect to the x-axis with the wave front parallel to the y-axis. However, these modes of P-wave and S-wave propagations are obviously not consistent with the particle motions produced by the incident shear wave such as

S_1 and S_0 mentioned above, which in fact is considered to be mainly responsible for most cases of severe ground vibrations.

As a sequel to Ref. 1, this study evaluates shear strains in the nonhomogeneous surface layer subjected to the incident shear waves S_0 and S_1 .

2. Shear Strain γ_1

Under the quasi-two-dimensional analysis considered here and also in Ref. 1, the normal strain ϵ_0 under S_0 and the shear strain γ_1 under S_1 are numerically equal if S_0 and S_1 are identical except for the direction of the particle motion. Indeed, one can show as in Ref. 1 that if the incident S_1 wave is assumed to be of the form

$$v_0 = \sqrt{2} \sum_{i=1}^n A_{0i} \cos(\omega_i t - k_{2i} z + \phi_i) \quad (4)$$

then, the displacement at the ground surface can be written as

$$v(H,t) = \sqrt{2} \sum_{i=1}^n \frac{2A_{0i}}{\sqrt{\cos^2 k_{1i} H + \alpha^2 \sin^2 k_{1i} H}} \cos(\omega_i t - \delta_i + \phi_i) \quad (5)$$

where

$$k_{1i} H = \omega_i H / V_1 \quad (6)$$

$$\delta_i = \tan^{-1} \frac{\alpha \sin k_{1i} H}{\cos k_{1i} H} \quad (7)$$

$$\alpha = \rho_1 V_1 / (\rho_2 V_2) \quad (8)$$

with H = thickness of surface layer, ρ_i = mass density and V_i = shear wave velocity ($i = 1$ for surface layer and 2 for the firm ground).

It is important to note that Eq. 4 represents, in the limit as $n \rightarrow \infty$, a stationary Gaussian random process² with zero mean and a one-sided spectral density $S_0(\omega)$ if

$$A_{0i} = \sqrt{S_0(\omega_i) \Delta\omega} \quad (9)$$

and ϕ_i are the random phase angles independently and uniformly distributed between 0 and 2π . In Eqs. 5, 6 and 9,

$$\omega_i = i\Delta\omega \quad (10)$$

and

$$\omega_n = n\Delta\omega \quad (11)$$

is the upper cut-off frequency beyond which the spectral density is assumed to be zero.

In the present study, the incident "acceleration" wave is assumed to have the one-sided spectral density of the following form.

$$S_A(\omega) = \frac{25\omega^2/289}{(1-\omega^2/242)^2 + \omega^2/289} \cdot \frac{100^2}{559} \quad (12)$$

This is the same analytical form as suggested in Ref. 3.

However, the parameter values are so adjusted that the spectral density will produce the standard deviation of 100 gal. Fig. 4 plots $S_A(\omega)$ in the range $\omega = 0$ to 200 rad/sec. The spectral density $S_O(\omega)$ of the displacement corresponding to Eq. 12 is obtained as $S_O(\omega) = S_A(\omega)/\omega^4$ with a truncation for the values of ω less than 0.6 rad/sec to make the standard deviation of the displacement process a finite value (in this case 2.1 cm). When the spectral density $S_O(\omega)$ is used in Eq. 5, the displacement $v(H,t)$ at the ground surface becomes a stationary Gaussian process with zero mean and the variance equal to

$$4 \sum_{i=1}^n S_O(\omega_i) \Delta\omega / (\cos^2 k_{1i}H + \alpha^2 \sin^2 k_{1i}H).$$

A sample function of the incident displacement wave given in Eq. 4 (with $z = 0$) is plotted over a stretch of 6.3 seconds in Fig. 5. For this purpose, Eqs. 4, 10, and 11 are used with $\Delta\omega = 0.6$ rad/sec, $\omega_n = 76.8$ rad/sec and hence $n = 128$.

Following the same reasoning as given in Ref. 1, the predominant frequency f_p is defined as

$$f_p = V_1/(4H) \quad (13)$$

and as mentioned earlier, it is assumed to be a random function of x ; $f_p = f_p(x)$. Because of Eq. 13, this implies that the shear velocity V_1 of the surface layer is also a random function of x ; $V_1 = V_1(x)$. As a first approximation, it is assumed that the predominant frequency is a stationary Gaussian process with

$$E[f_p(x)] = \mu_f \quad (14)$$

and

$$E[f_p(x)f_p(x + \xi)] = \bar{\sigma}_f^2 \phi(\xi) + \mu_f^2 \quad (15)$$

where ξ is the separation distance, $\bar{\sigma}_f$ is the standard deviation, and $\phi(\xi)$ is the normalized autocovariance function of the process. In the present study, the following form is used for $\phi(\xi)$;

$$\phi(\xi) = (1 - 2|\xi/L|^2) \exp\{-|\xi/L|^2\} \quad (16)$$

The Wiener-Khintchine transform of Eq. 15 with $\phi(\xi)$ given in Eq. 16 results in the one-sided spectral density $G(k)$ of $f_p(x)$.

$$G(k) = \frac{\bar{\sigma}_f^2 L^3 k}{2\sqrt{\pi}} \exp\{-k^2 L^2/4\} + 2\mu_f^2 \delta(k) \quad (17)$$

where $\delta(k)$ is the Dirac delta function. Equation 16 has been chosen for its simplicity, analytical tractability and possible compatibility with the reality, but mainly for the reason that

the derivative of $f_p(x)$ with respect to x exists at least in the mean square sense. Other significant characteristics that can be derived from Eqs. 16 and 17 are ω_a = apparent frequency (expected rate of positive zero crossing $\times 2\pi$), ν = expected rate of local maxima $\times 2\pi$, and $\epsilon = \omega_a/\nu$ = irregularity factor such that

$$\omega_a = \sqrt{6}/L, \nu = \sqrt{10}/L \text{ and } \epsilon = 0.77 \quad (18)$$

The normalized autocovariance function $\phi(\xi)$ is plotted in Fig. 6 while the spectral density $G(k)$ with $L = 100\text{m}$ in Fig. 7. The physical significance of L in Eqs. 16 and 17 is quite important; L has the dimension of length with a smaller value implying a shorter distance in which the correlation disappears. In the present study, the parameter L is called the "correlation distance" for convenience. If the degree of uniformity or homogeneity of the surface layer is termed "smoothness" as some researchers prefer, then the larger the correlation distance, the smoother the layer. To visualize this point, simulated sample functions of $f_p(x)$ in the form

$$f_p(x) = \sqrt{2} \sum_{i=1}^n B_{oi} \cos(k_i x + \phi_i) \quad (19)$$

with $L = 100\text{m}$ and 500m and of a length $1,000\text{m}$ are respectively shown in Figs. 8(a) and 9(a) with $\mu_f = 3.0 \text{ Hz}$ and $\overline{\sigma_f^2} = 0.5 \text{ Hz}^2$. Also, note that these figures have the V_1 scale corresponding to the f_p scale ($H = 20 \text{ m}$). As expected, a more rapid variation of f_p is observed in case of $L = 100 \text{ m}$ than in case of $L = 500 \text{ m}$. In Eq. 19,

$$B_{oi} = \sqrt{G(k_i) \Delta k} \quad (20)$$

with $k_i = i\Delta k$. The cut-off wave number $k_n = n\Delta k$ has the same significance as ω_n in Eq. 11, and ϕ_i are the random phase angles.

Although the correlation distance L does indicate the extent of the soil property variability as seen above, it is neither a direct nor familiar measure with which the degree of earthquake-induced damage of the underground pipelines can be associated. In the present study, the intensity of shear strain γ_1 that strictly results from the property variability of the surface layer is used as the measure of such variability to be correlated to the damage statistics.

Introducing the variability f_p into Eq. 5, one can write the displacement at the ground surface under the incident wave S_1 as

$$v(H,t,f_p) = \sqrt{2} \sum_{i=1}^n 2A_{0i}q_i^{-1/2} \cos\{\omega_i t + \theta_i\} \quad (21)$$

where A_{0i} is as given by Eq. 9,

$$q_i = \cos^2\left(\frac{\omega_i}{4f_p}\right) + \left(\frac{4Hf_p}{V_2}\right)^2 \sin^2\left(\frac{\omega_i}{4f_p}\right) \quad (\rho_1 = \rho_2) \quad (22)$$

and

$$\theta_i = -\tan^{-1}\left\{\frac{4Hf_p}{V_2} \sin\frac{\omega_i}{4f_p} / \cos\frac{\omega_i}{4f_p}\right\} + \phi_i \quad (23)$$

with ϕ_i being random phase angles as before. It is to be noted that Eq. 21 is now a function of t and f_p . Since f_p is a function of x , this means that $v(H,t,f_p)$ is also a function of x .

The shear strain γ_1 can then be written as

$$\gamma_1 = \frac{\partial v}{\partial x} = \frac{\partial v}{\partial f_p} \cdot r \quad (24)$$

where

$$r = df_p/dx \quad (25)$$

and

$$\frac{\partial v}{\partial f_p} = \sqrt{2} \sum_{i=1}^n 2A_{oi} \sqrt{E_i^2 + F_i^2} \sin[\omega_i t + \theta_i + \delta_i'] \quad (26)$$

with

$$E_i = \left\{ \omega_i \sin\left(\frac{\omega_i}{2f_p}\right) \left(\frac{2H^2}{V_2^2} - \frac{1}{8f_p^2} \right) - \frac{16H^2 f_p}{V_2^2} \sin^2\left(\frac{\omega_i}{4f_p}\right) \right\} / q_i^{3/2} \quad (27)$$

$$F_i = \frac{H}{V_2} \left(2 \sin \frac{\omega_i}{2f_p} - \frac{\omega_i}{f_p} \right) / q_i^{3/2} \quad (28)$$

and

$$\delta_i' = \tan^{-1}(E_i/F_i) \quad (29)$$

Then, it can be shown that

$$\overline{\left(\frac{\partial v}{\partial f_p} \right)^2} = \sum_{i=1}^n 4S_o(\omega_i) \Delta\omega (E_i^2 + F_i^2) \quad (30)$$

where a super bar indicates the temporal average. Since r is not a function of time, one can easily show that the temporal root mean square of the strain becomes

$$\sqrt{\overline{\left(\frac{\partial v}{\partial x} \right)^2}} = \sqrt{\overline{\left(\frac{\partial v}{\partial f_p} \right)^2}} \cdot |r| \quad (31)$$

Figures 8(b) and 9(b) show spatial distributions of the temporal root mean square strain corresponding to the variation of f_p as indicated in Figs. 8(a) and 9(a), respectively, assuming that $V_2 = 600$ m/sec. Then, the expectation of the temporal root mean square of the shear strain can be written as

$$E\left[\sqrt{\left(\frac{\partial v}{\partial x}\right)^2}\right] = \int_{-\infty}^{\infty} \int_{-\infty}^{\infty} \sqrt{\left(\frac{\partial v}{\partial x}\right)^2} g(f_p, r) df_p dr \quad (32)$$

where $g(f_p, r)$ is the joint density function of f_p and r . The expectation of Eq. 31 is equivalent to the spatial average of the temporal root mean square of the shear strain theoretically considered over the infinite domain $-\infty < x < \infty$ where the random variation of the predominant frequency is given by the stationary Gaussian process $f_p(x)$. Hereafter, the expectation indicated in Eq. 32 will be referred to as the "root mean square (RMS) shear strain" for simplicity.

Since the process is stationary and Gaussian, the joint density function $g(f_p, r)$ is given by

$$g(f_p, r) = \frac{1}{2\pi\bar{\sigma}_f\bar{\sigma}_r} \exp\left\{-\frac{(f_p - \mu_f)^2}{2\bar{\sigma}_f^2} - \frac{(r - \mu_r)^2}{2\bar{\sigma}_r^2}\right\} \quad (33)$$

where μ_f and $\bar{\sigma}_f$ are as defined in Eqs. 14 and 15, and

$$\mu_r = E[df_p/dx] = 0 \quad (34)$$

$$\bar{\sigma}_r^2 = \text{var}[df_p/dx] = 6 \bar{\sigma}_f^2 / L^2 \quad (35)$$

The last equation is obtained by making use of the following well known relationship;

$$\bar{\sigma}_r^2 \phi_r(\xi) = -\bar{\sigma}_f^2 d^2 \phi(\xi) / d\xi^2 \quad (36)$$

in which $\phi_r(\xi)$ is the normalized autocovariance of df_p/dx .

Substituting Eqs. 31 and 33 into Eq. 32 and carrying out the integration with respect to r , one obtains

$$E\left[\sqrt{\left(\frac{\partial v}{\partial x}\right)^2}\right] = \frac{\sqrt{6}}{\pi L} \int_{-\infty}^{\infty} \sqrt{\left(\frac{\partial v}{\partial f_p}\right)^2} \exp\left\{-\frac{(f_p - \mu_f)^2}{2\bar{\sigma}_f^2}\right\} df_p \quad (37)$$

To remove the difficulty associated with the assumption that $f_p(x)$ is a Gaussian process and therefore can take zero or any negative values, truncate the Gaussian density function at $f_p = f_{\min}$. This reflects the fact that the shear velocity V_1 of the surface layer physically cannot be too small. Writing V_{\min} for the smallest shear velocity value one can expect of the surface layer,

$$f_{\min} = V_{\min}/(4H) \quad (38)$$

the root mean square value given in Eq. 37 is modified as

$$E\left[\sqrt{\left(\frac{\partial v}{\partial x}\right)^2}\right] = \frac{\sqrt{6}}{\pi L} \int_{f_{\min}}^{\infty} \sqrt{\left(\frac{\partial v}{\partial f_p}\right)^2} \exp\left\{-\frac{(f_p - \mu_f)^2}{2\sigma_f^2}\right\} df_p / \left[1 - \Phi\left(\frac{f_{\min} - \mu_f}{\sigma_f}\right)\right] \quad (39)$$

where $\Phi(\cdot)$ indicate the standardized Gaussian distribution function.

The method by which Eq. 39 has been derived is exactly the same as that used in Ref. 1: Replacing u by v in the corresponding equations leads to the RMS value indicated in Eq. 39.

3. Shear Strain γ_0

As mentioned in the Introduction, the incident wave S_0 gives rise to the shear strain γ_0 in the x-z plane in the surface layer. It is important to note that, unlike $\epsilon_0 = \partial u / \partial x$ or $\gamma_1 = \partial v / \partial x$, γ_0 is not identically equal to zero even when the surface layer is perfectly homogeneous although it always vanishes at the ground surface or at $z = H$ because of the boundary conditions.

With a slight modification, the analysis in Ref. 1 can be extended to show that, under the incident wave S_0 , the displacement $u = u(H-z_0, t, f_p)$ in the randomly nonhomogeneous surface layer at a depth z_0 below the ground surface is

$$u(H-z_0, t, f_p) = \sqrt{2} \sum_{i=1}^n 2A_{0i} \cos(\omega_i z_0 / v_1) q_i^{-1/2} \cos(\omega_i t + \theta_i) \quad (40)$$

where A_{0i} , q_i and θ_i are respectively given by Eqs. 9, 22 and 23. Therefore, the shear strain γ_0 at $z = H-z_0$ is

$$\begin{aligned} \gamma_0(z_0) = \partial u(H-z_0, t, f_p) / \partial z_0 = & -\sqrt{2} \sum_{i=1}^n 2A_{0i} (\omega_i / v_1) \sin(\omega_i z_0 / v_1) \\ & \times q_i^{-1/2} \cos(\omega_i t + \theta_i) \end{aligned} \quad (41)$$

From Eq. 41, it follows that the temporal root mean square of $\gamma_0(z_0)$ is

$$\sqrt{\gamma_0^2(z_0)} = \sqrt{2} \sqrt{\sum_{i=1}^n 2A_{0i}^2 q_i^{-1} (\omega_i / v_1)^2 \sin^2(\omega_i z_0 / v_1)} \quad (42)$$

Finally, the expectation of the temporal root mean square can be derived as

$$E[\sqrt{\gamma_0^2(z_0)}] = \int_{-\infty}^{\infty} \sqrt{\gamma_0^2(z_0)} g_0(f_p) df_p \quad (43)$$

where $g_0(f_p)$ is the distribution function of f_p (at any value of x). If $g_0(f_p)$ is assumed to be Gaussian with mean μ_f and standard deviation $\bar{\sigma}_f$ truncated at $f_{\min} = V_{\min}/(4H)$ as before, then

$$E[\sqrt{\gamma_0^2(z_0)}] = \frac{1}{\sqrt{2\pi} \bar{\sigma}_f} \int_{f_{\min}}^{\infty} \sqrt{\gamma_0^2(z_0)} \exp\left\{-\frac{(f_p - \mu_f)^2}{2\bar{\sigma}_f^2}\right\} df_p / [1 - \Phi\left(\frac{f_{\min} - \mu_f}{\bar{\sigma}_f}\right)] \quad (44)$$

It is to be noted that $\gamma_0(z_0)$ does not depend on the correlation distance L , and that $\gamma_0(z_0)$ and $\gamma_1(z_0) = \partial v / \partial z|_{z=H-z_0}$ are numerically identical, as ε_0 and γ_1 are, if the incident waves S_0 and S_1 are identical except for the direction of their particle motions.

4. Correlation Between the Shear Strain and the Damage Statistics

In one of the recent Japanese studies⁴, the ground predominant frequencies are evaluated at the nodal points of a grid of meridians and parallels (both at intervals of 1 km) covering the Tokyo metropolitan area. The evaluation is made based on the soil conditions at the nodes under the shear beam assumption, and for each area element of 1 km², the average f^* and the standard deviation σ_f^* of the predominant frequency are computed using the frequencies evaluated at its four corners.

The study⁴ then examines the (old but still valid) statistics taken on the underground water supply pipeline system which was in service at the time of the 1923 Kanto Earthquake and counts the number of pipe breaks and leakages in each area element resulting from the same earthquake. These numbers are divided by the length (in km) of the pipelines in each area to obtain the "break damage index" D or the "leakage damage index". Furthermore, the study correlates f^* and σ_f^* to D by dividing the f^* and σ_f^* space into the following four regions as shown in Table 1.

Table 1. Break Damage Index for Four Regions

	f^*	σ_f^*	\bar{D}
I	1.5 ~ 3.5	0 <	5.1
II	3.5 ~ 4.5	0 ~ 1.15	2.6
III	3.5 ~ 4.5	1.15 <	13.3
IV	4.5 ~ 5.5	0 <	2.8

The quantity \bar{D} in Table 1 indicates the average value of D in each region. Table 1 shows that region III produces the worst damage statistics while region I is the second worst. The damage indices associated with regions II and IV are much smaller than that with region III.

These Japanese data implicitly assume that the variation of the predominant frequency is two-dimensional, i.e., $f_p = f_p(x,y)$. Although it is not extremely difficult to deal with such two-dimensional random processes, as done in Ref. 5, the amount of numerical effort required to do so would be inconsistent with the quality and quantity of the available field data. Therefore, as seen in the preceding sections, the present investigation deals with the case where the predominant frequency f_p varies only in the x direction, i.e., $f_p = f_p(x)$ and where f_p is evaluated along the x axis at equal intervals of 1 km. This is a one-dimensional equivalent of the Japanese study such that the predominant frequency in each interval of 1 km varies as a random process $f_p(x)$ characterized by Eqs. 14-17, with a value L common to all the intervals but with a set of values of μ_f and $\bar{\sigma}_f$ unique to that interval. Under these circumstances, it is considered as a first approximation that μ_f and $\bar{\sigma}_f$ to be used for an interval are equal respectively to the sample mean and the sample standard deviation obtained on the basis of the predominant frequencies evaluated at both ends of that interval.

For $L = 300\text{m}$, $H = 20\text{ m}$, $V_2 = 600\text{m/sec}$ and $V_{\min} = 50\text{m/sec}$, Fig. 10 is obtained which indicates the root mean square (RMS)

shear strains (Eq. 39) for various combinations of μ_f and $\bar{\sigma}_f$; $\mu_f = .75, 1.25, 1.75, \dots, 6.75$ Hz and $\bar{\sigma}_f = .125, .375, .625, \dots, 3.125$ Hz. Purely for the purpose of establishing the trend, it is assumed that a particular combination of f^* and σ_f^* under the assumption of two-dimensional variation of f_p will produce the same RMS surface strain as those obtained in Fig. 10. Fig. 10 is then used in conjunction with the Japanese data⁴, particularly with those given in Fig. 11 showing the numbers of the area elements of 1 km square associated with indicated combinations of f^* and σ_f^* with blanks implying zero; $f^* = .75, 1.25, 1.75, \dots, 6.75$ Hz and $\sigma_f^* = .125, .375, .625, \dots, 3.125$ Hz (these values are the same as for μ_f and $\bar{\sigma}_f$). Thus, the $\mu_f(f^*) - \bar{\sigma}_f(\sigma_f^*)$ plane in Fig. 10 can be divided into four regions, I, II, III, and IV as defined in Table 1.

The weighted averages of the RMS shear strains γ_1 within regions I-IV are then computed with the numbers shown in Fig. 11 as weight. These averages, which will be referred to as the "regional RMS shear strains" are also shown in Fig. 10. The same computations are repeated for $L = 500$ m, 800 m, 1,000 m and 2,000 m resulting in five sets of four regional RMS strain values as indicated in Fig. 12(a) in terms of a bar graph. Fig. 12(a) shows that the regional RMS shear strains γ_1 are larger for smaller values of L within individual regions as expected, and that the largest value is observed in region III, the second largest in region I, the third in region IV and the smallest in region II for the same value of L . The latter result

exhibits the same trend observed in the Japanese data⁴ in Table 1 and Fig. 12(b) demonstrating how the break damage index depends on the region. The trend is even more similar if one considers the following: assuming a larger value of L for region I than for other regions may be more appropriate since the soil conditions of region I are generally those of alluvium and are expected to be more homogeneous than in other regions where the loam generally combined with the river valley humic soil dominates. For example, take the RMS values associated with $L = 500$ m for region I while the RMS values with $L = 300$ m for other regions, and observe how closely the results compare with that of Fig. 12(b).

Similar computations are made for the RMS value of shear strain γ_0 (Eq. 43) at $z_0 = 0.5$ m, 1.0m and 2.0m for the same combinations of μ_f and $\bar{\sigma}_f$ as for γ_1 and are shown in Figs. 13, 14, and 15, respectively. As mentioned earlier, γ_0 is independent of the correlation distance L and Figs. 13-15 indicate that the influence of the random nonhomogeneity on γ_0 is much less than in the case of γ_1 .

The regional RMS strain values are also computed for γ_0 in the same way as for γ_1 and shown in terms of a bar diagram in Fig. 16. The diagram shows that for the incident shear wave S_0 considered here, the RMS values are larger for larger values of z_0 or at deeper locations and more importantly that the largest RMS value is observed for Region I followed by those in III, II and IV in that order. This last observation indicates that the correlation between the damage statistics as

shown in Fig. 12(b) and the RMS shear strain values for γ_0 are not as significant as for γ_1 or ϵ_0 .

Finally, it is pointed out that, because of the numerical identity between γ_0 and γ_1' as mentioned earlier, the bargraph for the regional RMS values in Fig. 16 serves for γ_1' as well as for γ_0 .

5. Conclusion

The shear strains in the surface layer of randomly non-homogeneous property are evaluated under the quasi-two-dimensional assumptions. The shear strain γ_0 in the x-z plane due to the incident shear wave S_0 with the particle motion in the direction of the x-axis and the shear strain γ_1 in the x-y plane due to the incident shear wave S_1 with the particle motion in the direction of the y-axis are considered. The RMS values of these strains are compared with the statistics of earthquake-induced damage based on a field study on the underground water supply pipelines in Tokyo. The comparison indicates that a good correlation exists between the RMS values for γ_1 and the degree of the damage, while the correlation is not as good for γ_0 .

6. Acknowledgement

This work was supported by the National Science Foundation under Grant No. ENV-76-09838 (Prime Contractor, Weidlinger Associates; Subcontractor, Columbia University). The authors are grateful to Professors K. Kubo and T. Katayama of the University of Tokyo for providing us with the valuable damage statistics and other information. They are also grateful to Messrs. P. Weidlinger, M. Baron and J. Wright of Weidlinger Associates for their suggestions and discussions throughout the investigation.

References

1. Shinozuka, M. and Kawakami, H., "Underground Pipe Damages and Ground Characteristics", Technical Report No. CU-1 under NSF Grant No. ENV-76-09838; presented at the Lifeline Earthquake Engineering Specialty Conference at the University of California, Los Angeles, August 30-31, 1977.
2. Shinozuka, M., "Digital Simulation of Random Processes in Engineering Mechanics with the Aid of FFT Technique", in "Stochastic Problems in Mechanics", edited by Ariaratnam, S.T. and Leipholz, H.H.E., University of Waterloo Press, 1974, pp. 277-286.
3. Newmark, N.M. and Rosenblueth, E., "Fundamentals of Earthquake Engineering", Prentice-Hall, 1971, p. 291.
4. Kubo, K. and Katayama, T., "Survey on Underground Pipe Damages due to Earthquake", Tokyo Metropolitan Disaster Prevention Congress, Governor's Office, The Metropolitan Government of Tokyo (in Japanese).
5. Shinozuka, M. and Lenoë, E., "A Probabilistic Model for Spatial Distribution of Material Properties", J. Engineering Fracture Mechanics, Vol. 8, 1976, pp. 217-227.

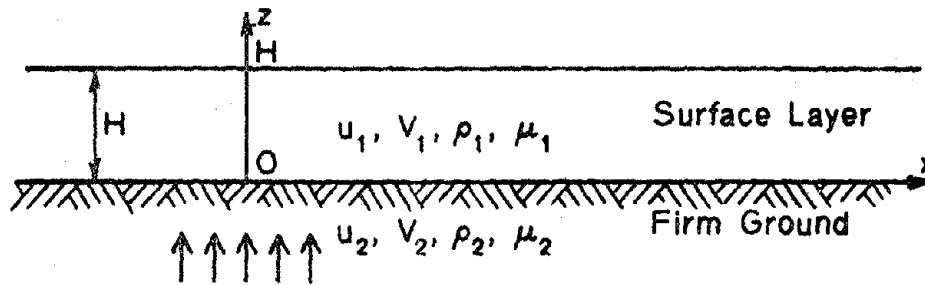


Fig. 1 Ground Model.

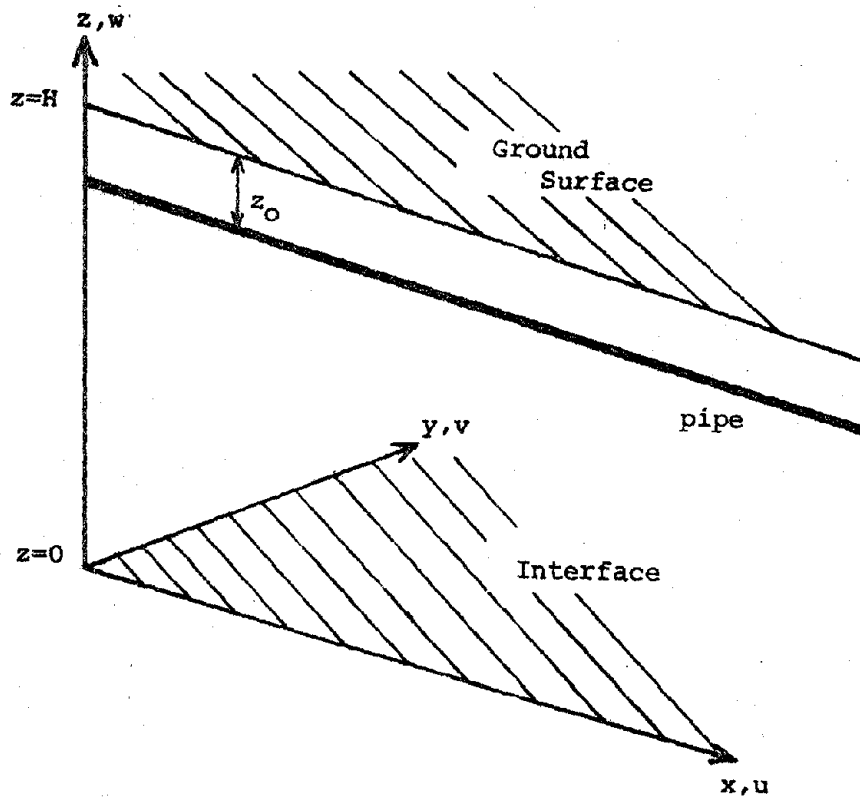


Fig. 2 Coordinate system

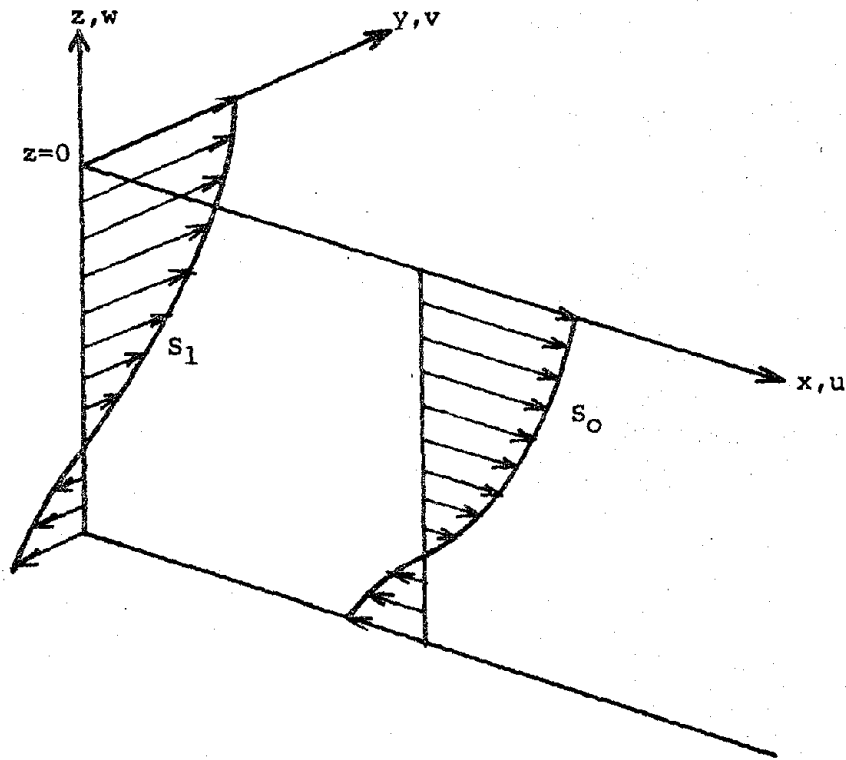


Fig. 3 Incident shear waves

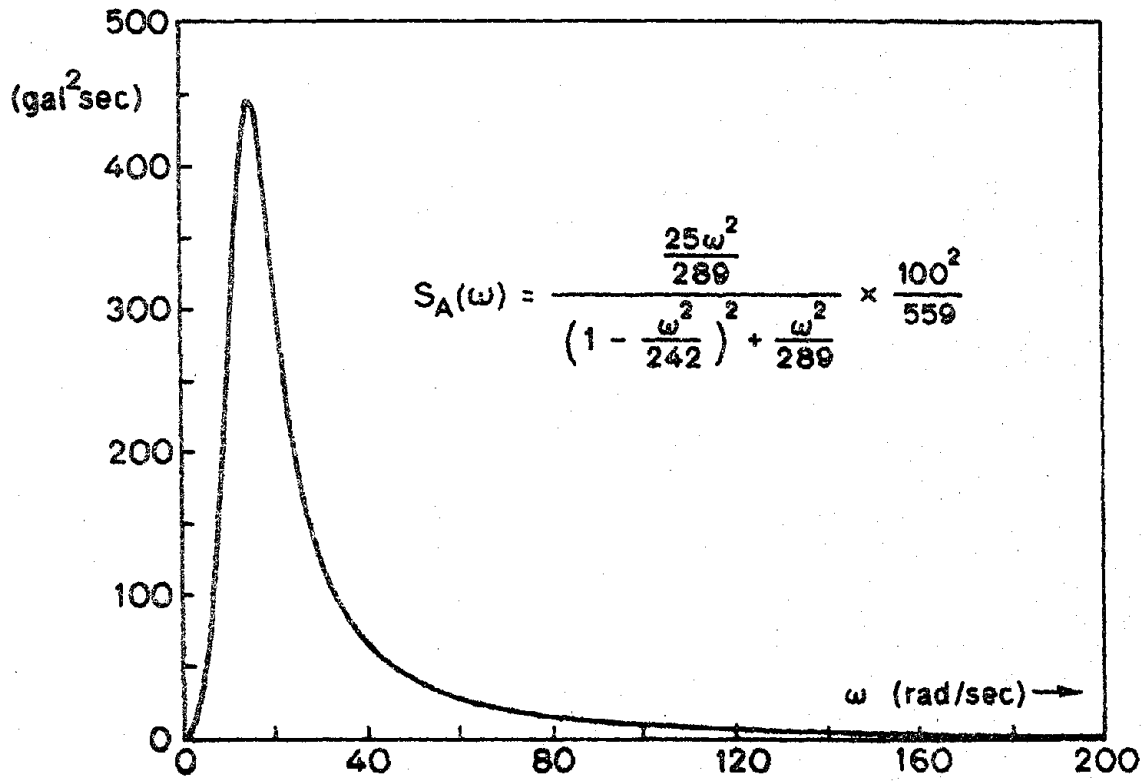


Fig. 4 Power Spectral Density (Acceleration).

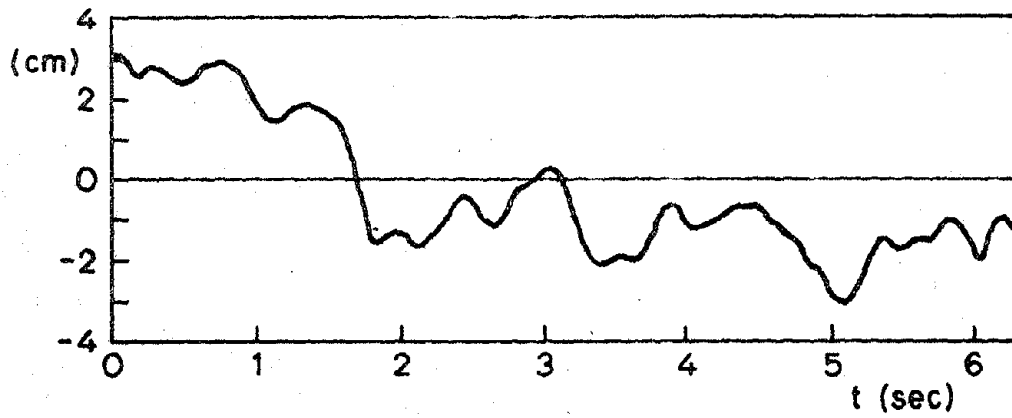


Fig. 5 Incident Wave.

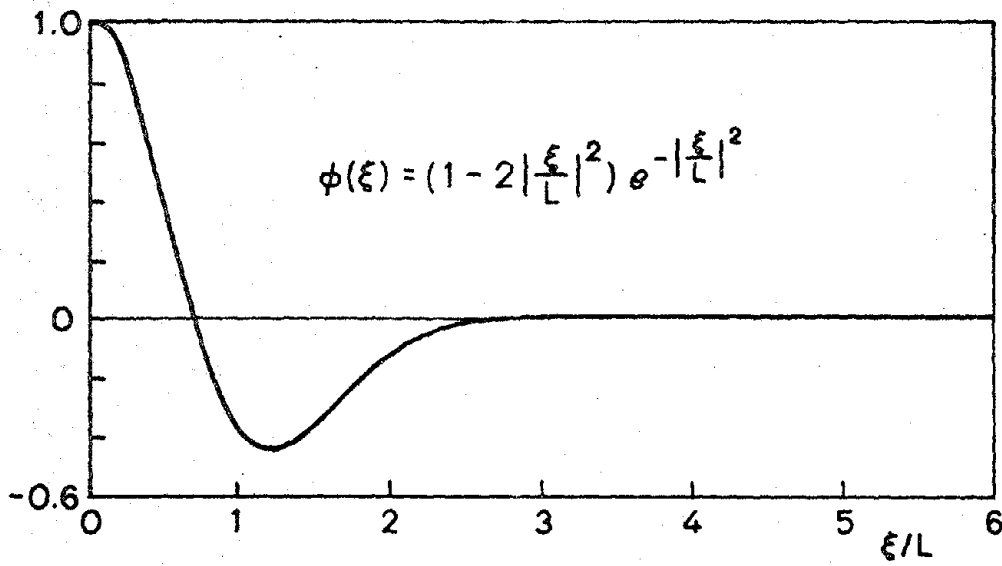


Fig. 6 Spatial Auto-Covariance (normalized).

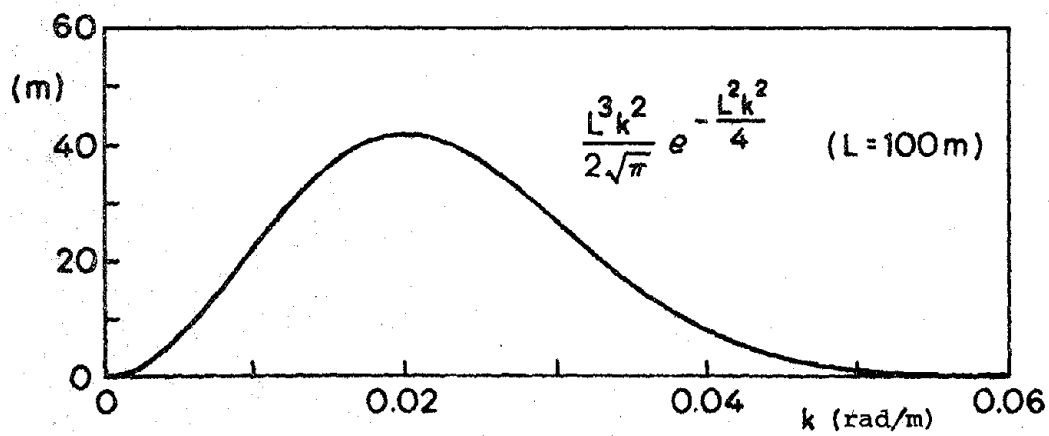


Fig. 7 Spatial Power Spectral Density.

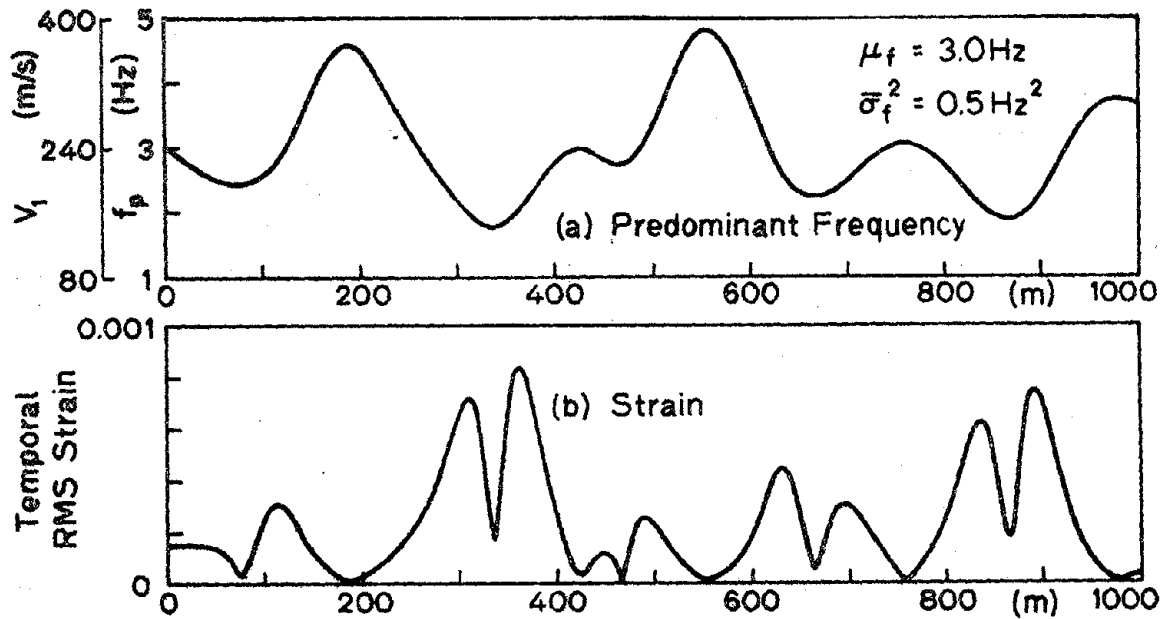


Fig. 8 Spatial Variation of Predominant Frequency and Shear Strain γ_1 ($L = 100$ m).

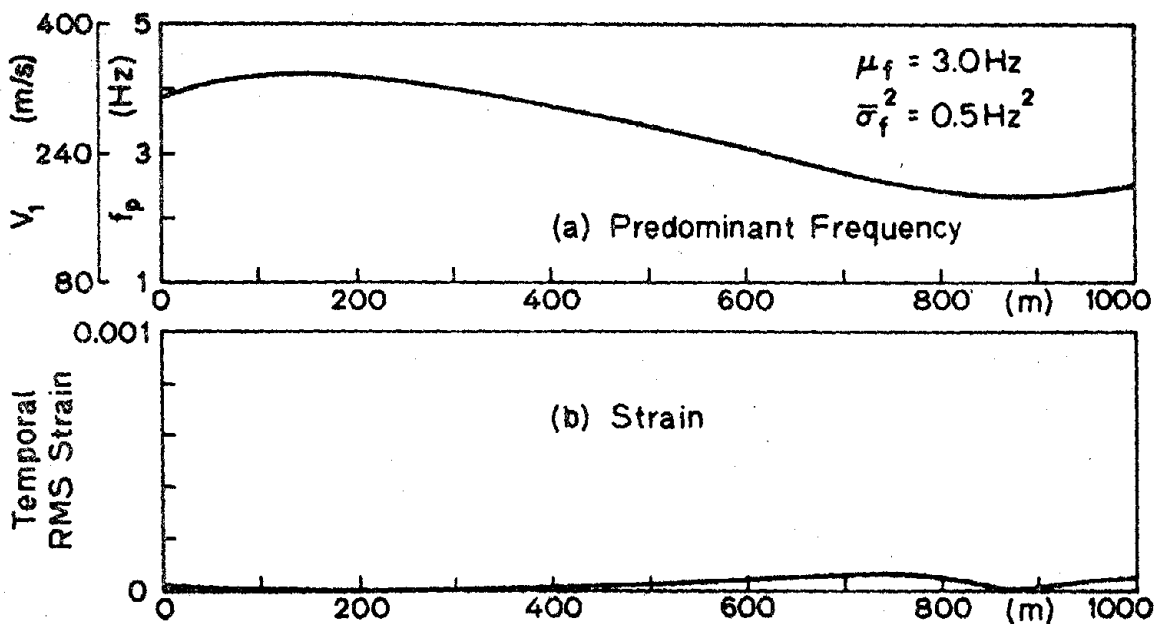


Fig. 9 Spatial Variation of Predominant Frequency and Shear Strain γ_1 ($L = 500$ m).

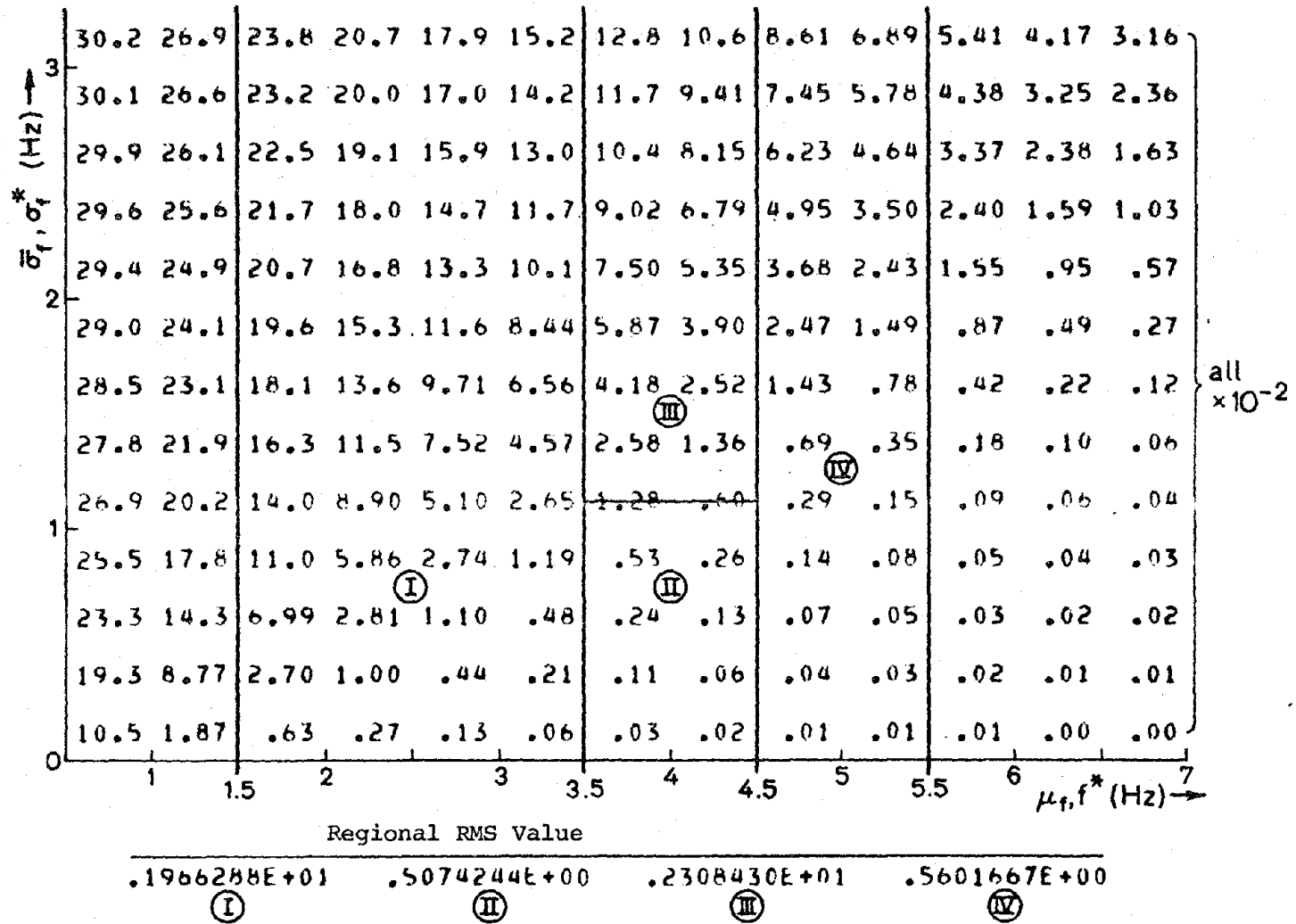


Fig. 10 RMS Shear Strain γ_1 (L = 300 m, $V_{min} = 50$ m/s).

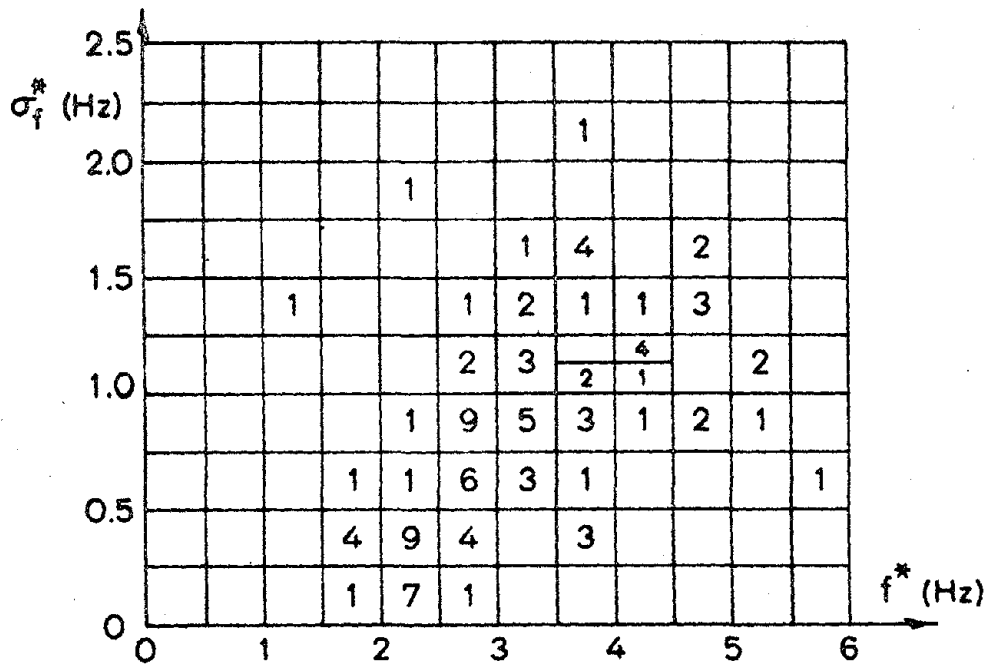


Fig. 11 Frequency Distribution of f^* - σ_f^* Combinations.

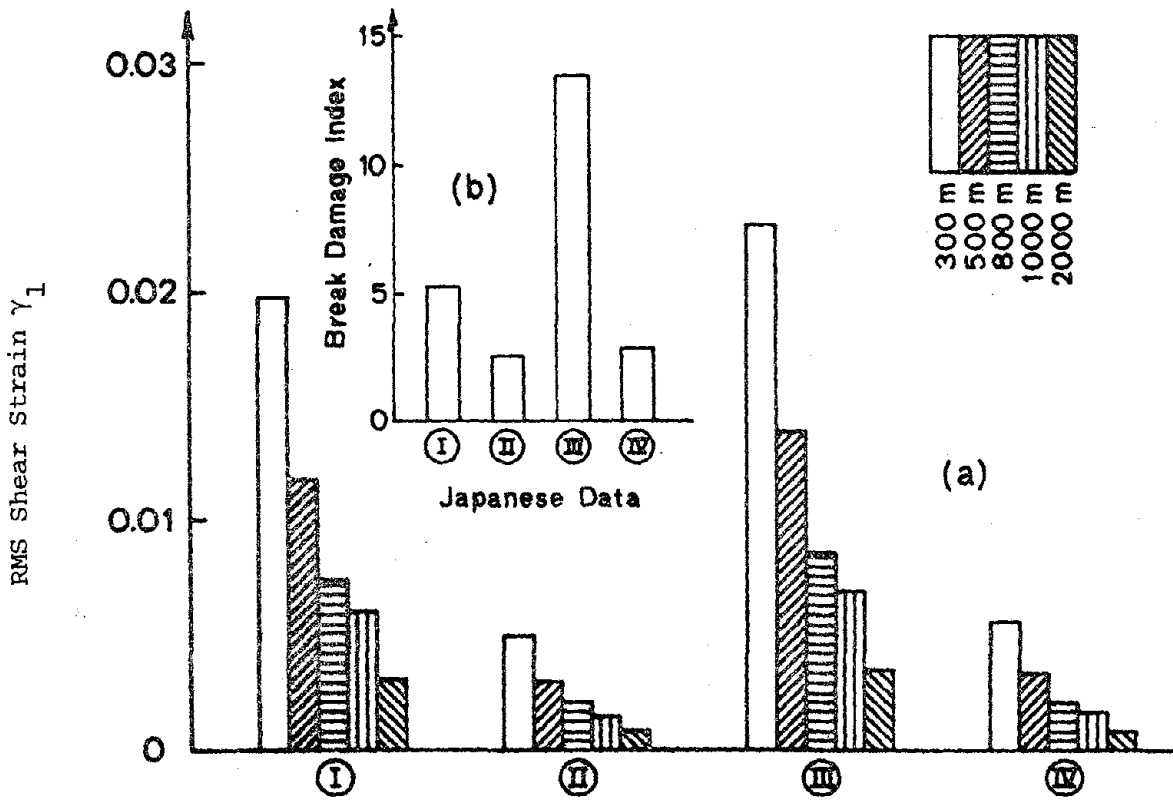
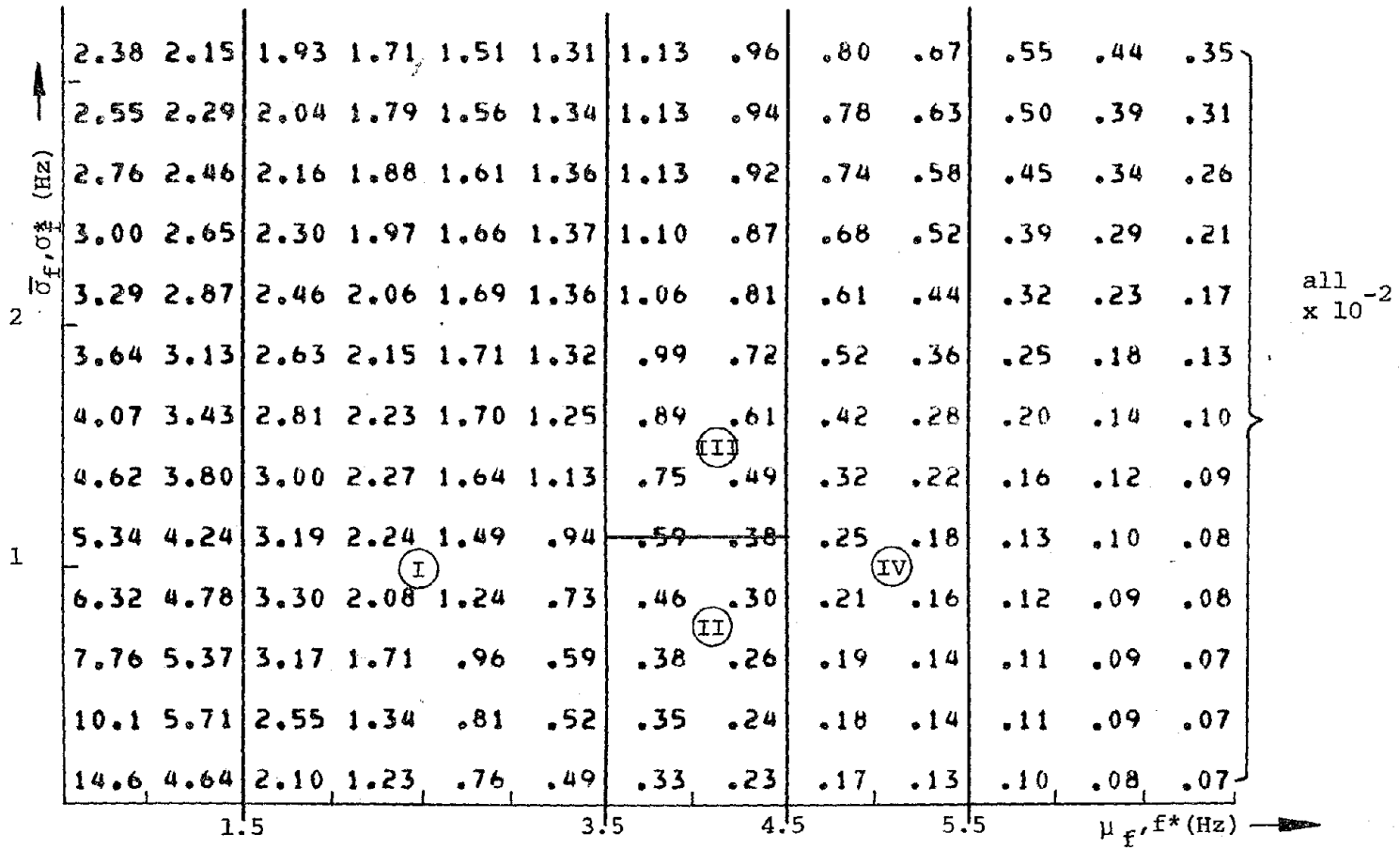


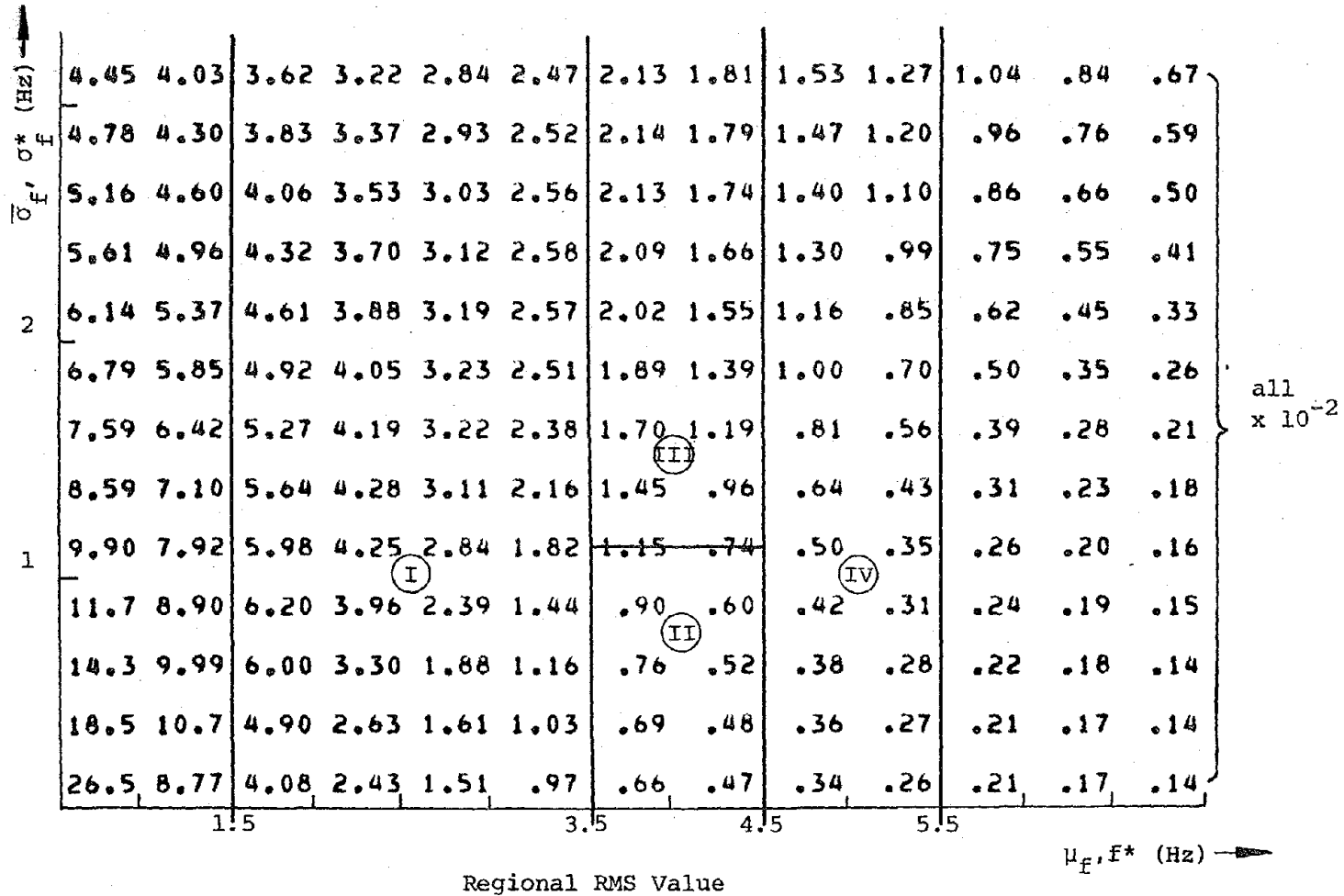
Fig. 12 Regional RMS Shear Strain γ_1 .



Regional RMS Value

.1265735E+01	.4232109E+00	.6305033E+00	.2743366E+00
I	II	III	IV

Fig. 14 RMS Shear Strain γ_0 ($z_0 = 1.0$ m, $V_{min} = 50$ m/sec).



.2457991E+01	.8350201E+00	.1218892E+01	.5393944E+00
I	II	III	IV

Fig. 15 RMS Shear Strain γ_0 ($z_0 = 2.0$ m, $V_{\min} = 50$ m/sec).

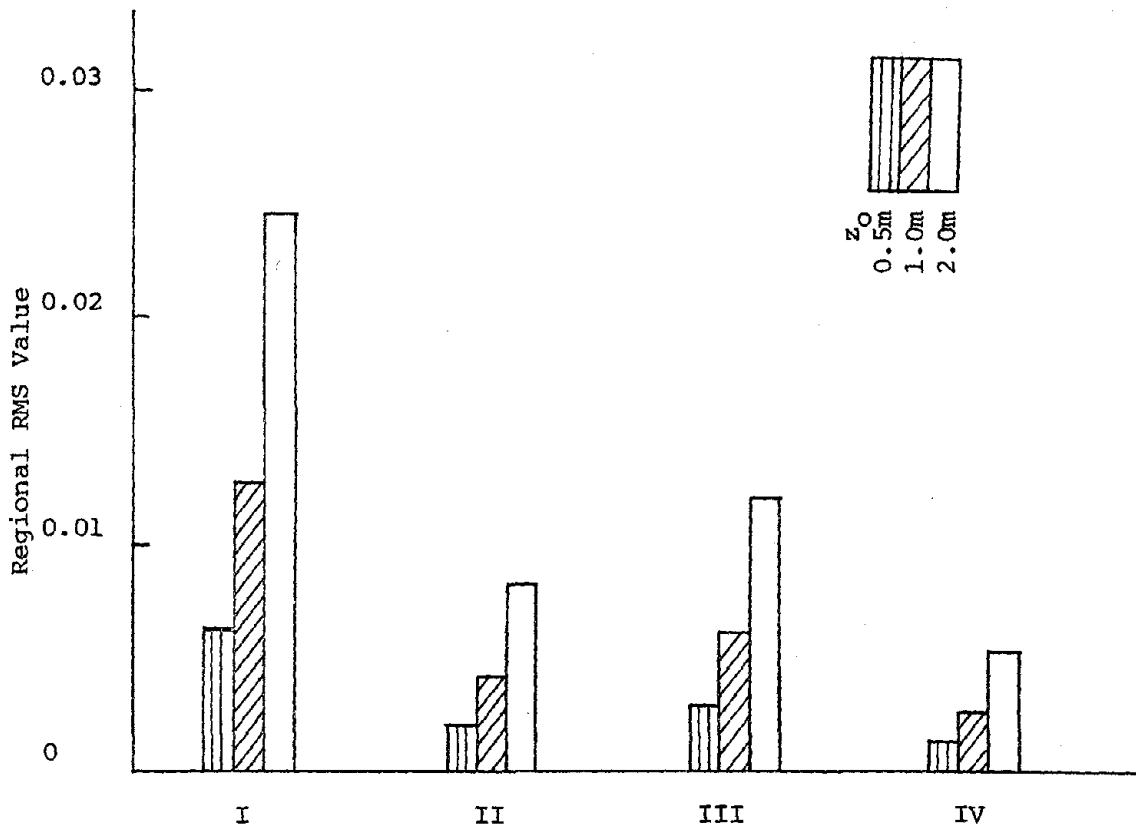


Fig. 16 Regional RMS Shear Strain γ_0 .

